Clays and Clay Minerals, Vol. 60, No. 1, 1–17, 2012.

LOW-TEMPERATURE HYDROTHERMAL METAMORPHIC MINERALIZATION OF ISLAND-ARC VOLCANICS, SOUTH APUSENI MOUNTAINS, ROMANIA

GEORGE DAN MIRON[1,2,*], PHILIP S. NEUHOFF[3], AND GEORG AMTHAUER[4]

[1] Department of Earth Sciences, ETH Zürich, Sonneggstrasse 5, 8092 Zürich, Switzerland
[2] Department of Geology, Babeş–Bolyai University, Kogălniceanu 1, 400084 Cluj-Napoca, Romania
[3] Department of Geological Sciences, University of Florida, 241 Williamson Hall, Gainesville, Florida 32611-2120, USA
[4] Department of Material Sciences, University of Salzburg, Hellbrunnerstrasse 34, 5020 Salzburg, Austria

Abstract—The island-arc volcanics situated in the eastern part of the Căpîlnaş-Techereu nappe (South Apuseni Mountains, Romania) were studied to evaluate the temperature, fluid properties, and mineral chemistry during low-temperature metamorphism. Detailed observations of metamorphic mineral assemblages were conducted using powder X-ray diffraction and electron microprobe. The metamorphism involved albitization of plagioclase feldspar and the formation of mafic phyllosilicates, zeolites, and other hydrous Ca-Al-silicate minerals. Mafic phyllosilicates consisted of transitional dioctahedral-trioctahedral smectites, mixed-layer chlorite-smectite (C/S, 6–96% chlorite), and discrete chlorite. The zeolites were analcime, stilbite ± stellerite, heulandite, laumontite, epistilbite, and mordenite. Also present, as secondary minerals filling amygdales and veins, are prehnite, pumpellyite, and secondary amphibole. Two mineral assemblages were identified which provide important information about metamorphic conditions (temperature, reaction progress, and fluid properties): (1) heulandite + analcime + quartz; and (2) laumontite + albite + quartz + prehnite + pumpellyite ± amphibole. The types of and relations between minerals in the first assemblage suggest the occurrence of low-temperature hydrothermal metamorphism in the zeolite facies at ~125ºC, whereas the second assemblage was metamorphosed at 200ºC. The composition and variability of the mineral assemblages in the study area suggest that, due to slow reaction rates, the low-temperature transformations and mineral assemblages were influenced not only by temperature but also by local rock composition, fluid-rock ratio, and fluid chemistry.

Key Words—Chlorite/smectite, Low-temperature Hydrothermal Metamorphism, Prehnite, Pumpellyite, Romania, South Apuseni Mountains, Zeolites.

INTRODUCTION

Secondary mineral assemblages can provide an important record of the post-emplacement metamorphic processes and conditions (temperature, fluid physico-chemical properties, and bulk-rock chemistry) that modify igneous rocks. Mafic phyllosilicates are common in basic and intermediate igneous rocks metamorphosed under very low-grade and low-grade metamorphic conditions. These phyllosilicates are often associated with zeolites and other hydrous Ca-Al silicates (*i.e.* prehnite, pumpellyite, epidote, and actinolite). The presence of different mineral assemblages can be used to constrain metamorphic facies (Cho *et al.*, 1986; Liou *et al.*, 1987; Bevins *et al.*, 1991a; Cho, 1991; Inoue and Utada, 1991; Dekayir *et al.*, 2005; Marantos *et al.*, 2008). Zeolites are characteristic of the lowest metamorphic grade. Zeolites destabilize with increasing temperature. Their absence, combined with the presence of prehnite, pumpellyite, and epidote, characterize the prehnite-pumpellyite facies (Cho *et al.*, 1986; Cho, 1991; Bevins *et al.*, 1991b). In the case of actinolite present with prehnite or with pumpellyite, the metamorphic facies becomes prehnite-actinolite or pumpellyite-actinolite. The transition of smectite to chlorite is another indicator of increasing metamorphic grade. The reaction typically does not attain thermodynamic equilibrium (Merriman and Peacor, 1999; Árkai *et al.*, 2000) and is manifested by chlorite/smectite (C/S) irregularly mixed layering (*e.g.* Bettison *et al.*, 1991; Schiffman and Fridleifsson, 1991; Robinson and Bevins, 1994; Meunier *et al.*, 2008a; Meunier *et al.*, 2008b; Leoni *et al.*, 2010) or by discontinuous changes from smectite to corrensite to chlorite without irregularly mixed-layered chlorite/smectite (*e.g.* Shau *et al.*, 1990; Schiffman and Staudigel, 1995; Schmidt and Robinson, 1997). Variations in temperature (Chipera and Apps, 2001; Utada, 2001) and compositions of bulk rock and fluid can lead to mineral compositional variations within each facies (Liou *et al.*, 1987; Springer *et al.*, 1992; Beiersdorfer, 1993; Bevins and Robinson, 1993; Digel and Ghent, 1994; Day and Springer, 2005; Robinson *et al.*, 2005; Muñoz, 2010) and shifts in temperature-pressure space of the zeolite, prehnite-pumpellyite, and prehnite-actinolite facies, making it difficult to assign a characteristic facies to the rocks.

* E-mail address of corresponding author:
mirondanro@yahoo.com
DOI: 10.1346/CCMN.2012.0600101

No research has been done, to date, in the study area and in the whole South Apuseni island-arc volcanic rocks, dealing with a detailed description of the secondary mineralization and using it to constrain the metamorphic-facies conditions. A synthesis on the metamorphism and related processes that affected the Alpine ophiolites and the associated island-arc volcanic rocks in the South Apuseni Mountains was published by Savu (1996). He divided the metamorphic processes as follows: intra-crustal (late-magmatic hydrothermal and contact metamorphism), supra-crustal (diagenesis and ocean-floor metamorphism), and post ocean-closure (dynamic, dynamo-thermal, and burial metamorphism). Ellero *et al.* (2002) determined the metamorphic grade in the lower tectonic unit (Feneş nappe, consisting of sedimentary rocks) using mineral paragenesis and the 'crystallinity' of illite and chlorite. The results from Ellero *et al*. (2002) revealed that the rocks were transformed under late diagenetic to diagenetic-zone/anchizone boundary conditions.

The aim of the present study was to assess the low-temperature transformations and the geological controls (temperature, fluid properties, rock composition) on the mineral assemblages, by detailed examination of the secondary mineralization, *i.e.* mafic phyllosilicates and hydrous Ca-Al silicates, using the approach of interpreting compositional variations of phases, incomplete mineral reactions, and contrasting assemblages.

GEOLOGICAL SETTING

The study area (Figure 1) located in the South Apuseni Mountains, Romania, part of the Carpathian Belt, is bounded by the Balşa-Techereu-Poieniţa villages. Most of the South Apuseni Mountains are interpreted as a suture zone between Tisia and the Euroasiatic plates (Savu, 1983). The lithostratigraphy reflects early extension followed by subduction at the end of the Jurassic. The main lithologies include: a lower ophiolitic sequence and overlying calc-alkaline series belonging to the late Jurassic island arc (Savu, 1983; Savu *et al.*, 1994; Saccani *et al.*, 2001; Bortolotti *et al.*, 2002; Hoeck *et al.*, 2009; Ionescu *et al.*, 2009), all deformed *via* nappe stacking from Early Aptian to Late Maastrichtian. Rocks in the study area are part of the Căpîlnaş-Techereu nappe (also known as the Mureş nappe), which is the upper-most nappe in the sequence, overlying the Feneş nappe (Ellero *et al.*, 2002). Volcanics exposed within the study area are associated with the youngest arc activity and are mainly basalts and basaltic-andesites with plagioclase feldspar and/or pyroxene phenocrysts. Associated with these are pyroclastic deposits (Savu *et al.*, 1986; Savu and Udrescu, 1996).

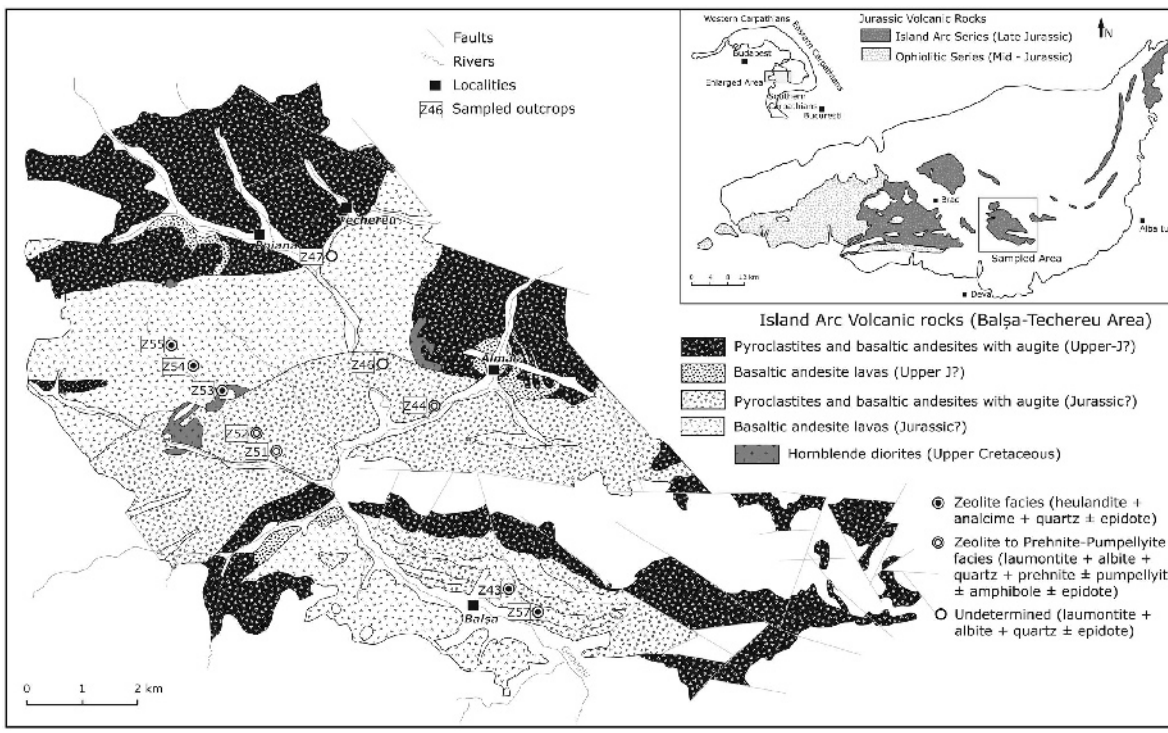

Figure 1. Simplified geological sketch-map of the Balşa–Techereu–Poiana (Poieniţa) area (modified after the Romanian Geological Map, section 74c, Zlatna (1:50,000)). The location of the sampled area within the South Apuseni Mountains, the locations of the outcrops sampled, and the metamorphic facies are shown.

https://doi.org/10.1346/CCMN.2012.0600101 Published online by Cambridge University Press

ANALYTICAL METHODS

Samples were collected from 10 outcrops (Table 1, Figure 1) of the lava flows and pyroclastic deposits. Thin sections were examined in transmitted light to establish mineral assemblages and phase relations. Powder X-ray diffraction (XRD) and electron probe microanalysis (EPMA) were used to determine the mineral phases and their chemical composition (major oxide concentrations). The XRD patterns were recorded using an automated diffractometer (Siemens D500, University of Salzburg, Austria) with CuKα radiation (40 kV, 45 mA) between 3 and 75º2θ (step size 0.02º2θ with a measuring time of 6 s per step). The program *EVA* 3.0 (part of the software package *Diffrac Plus* from BRUKER AXS) including the PDF-2 database (2009 release, International Centre for Diffraction Data) was used to evaluate the diffraction data. Mineral chemistry was determined by EPMA using a JEOL 8600 electron microprobe (University of Salzburg, Austria) operated at 15 kV accelerating potential and 30 nA beam, with a 10 μm beam diameter. Calibration was conducted using synthetic standards SiO_2, Al_2O_3, MgO, NaCl, KCl, TiO_2, FeO, and MnO (reference standards for X-ray Microanalysis from Micro-Analysis Consultants Ltd., St. Ives, Cambridgeshire, UK), and a natural standard wollastonite for Ca. A ZAF (Z – atomic number; A – absorption; F – fluorescence) matrix correction was applied. The structural formula for the phyllosilicates analyzed was recalculated based on a chlorite formula with the total cation charge of 44, *i.e.* neutralizing the equivalent of 28 oxide ions. Chlorite being an end member in the chlorite–smectite transition would have 20 non-interlayer cations in its pure form, while end-member trioctahedral smectite would have 17.8, and the end-member for dioctahedral smectite would have 15.2 (Schiffman and Fridleifsson 1991; Robinson *et al.*, 1993). The percentage of chlorite in C/S (mixed-layer chlorite/smectite) was estimated from EPMA of the total molar Si+Al+Mg+Fe content of the minerals by linear interpolation between smectite and chlorite end members (after Schiffmann and Fridleifsson, 1991).

RESULTS

Primary mineralogy

Primary plagioclase phenocrysts, although readily identified in thin section, had been replaced extensively by albite, zeolites, and mafic phyllosilicates. In most of the samples studied, former plagioclase phenocrysts were nearly albitic in composition with anorthite mole fractions of <2.5% (Table 1). Albitization is often zoned, with intracrystalline regions of pristine or partially albitized plagioclase present in otherwise albitized grains. In outcrops Z57 and Z43, plagioclase was not completely pseudomorphed by albite, but was often found as relict or replaced by heulandite and C/S phyllosilicates (Figure 2a).

In addition to plagioclase, unaltered K-feldspar phenocrysts (Table 2) and clinopyroxene (augite) pheno-

Table 1. Outcrops sampled and the minerals identified.

	Z43	Z44	Z46	Z47	Z51	Z52	Z53	Z54	Z55	Z57
Albite	X[a]	X[a]			X[a]	X[a]			X[a]	X[a]
Epistilbite	X[b]							X[b]		
Stilbite	X[b]						X[b]		X[b]	X[b]
Mordenite	X[b]									
Analcime									X[b]	X[a,b]
Heulandite	X[a,b]								X[a,b]	X[a,b]
Laumontite		X[a,b]	X[b]	X[b]	X[a,b]		X[b]			
Prehnite		X[a,c]			X[a,c]					
Pumpellyite		X[a,c]			X[a,c]					
Epidote	X[c]		X[c]	X[c]	X[a,c]	X[a,b,c]	X[b,c]	X[c]	X[c]	
Amphibole					X[a,c]					
Glauconite										X[a,c]
C/S	X[a,b,c]	X[a,b,c]	X[b,c]	X[b,c]	X[a,b,c]	X[a,b,c]	X[b,c]	X[c]	X[a,b,c]	X[a,b,c]
Calcite	X[b,c]		X[b,c]			X[c]	X[b,c]	X[c]		
$X^{d}_{anorthite}$	2–80	<3			4–12	<3			<3	57–73
% chlorite[e]	6–96	45–6			36–7	63–90			26–72	30–8
	σ = 25.41	σ = 5.54			σ = 12.01	σ = 7.53			σ = 14.41	σ = 26.15

[a] believed to be present from use of EPMA
[b] identified using XRD
[c] identified using optical microscopy
[d] mole fraction of anorthite in plagioclase
[e] percentage of chlorite interlayers in C/S
σ – standard deviation

https://doi.org/10.1346/CCMN.2012.0600101 Published online by Cambridge University Press

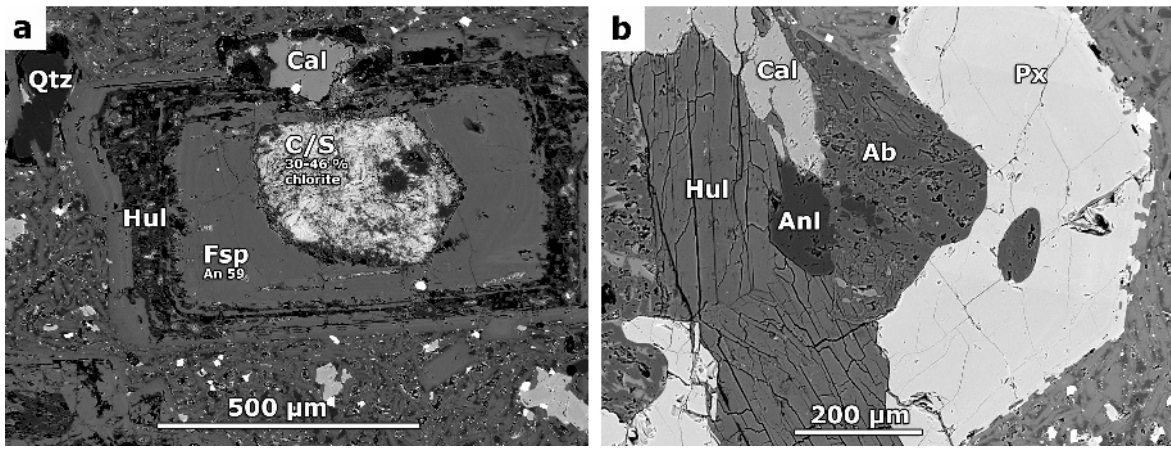

Figure 2. Backscattered electron (BSE) images from outcrop Z57: (a) plagioclase feldspar (Fsp) being replaced by heulandite (Hul) with C/S part of a previously mafic magmatic mineral. (b) Sample with analcime (Anl) together with heulandite (Hul), calcite (Cal), albite (Ab), and clinopyroxene (Px).

crysts are present. The clinopyroxene (augite) was barely altered and was of almost uniform chemical composition with Ca, Mg, and Fe having values of 0.77–0.87, 0.83–0.89, and 0.13–0.25 atoms per formula unit (a.p.f.u.), respectively. K-feldspars showed albite replacements at crystal rims.

Metamorphic minerals

Extensive replacement of primary phases by secondary minerals was observed throughout the samples. The rocks had a porphyritic texture with a microfelsitic to fine-grained matrix. Phenocrysts and much of the groundmass were replaced by low-temperature meta-

Table 2. Representative compositions of 'replaced' and 'fresh' plagioclase, recrystallized* secondary albite in amygdales, and K-feldspar (Kfs) determined by means of EPMA.

Outcrop	Z43 'replaced'	Z44 'replaced'	Z51 'replaced'	Z51 *	Z55 'replaced'	Z52 'replaced'	Z57 'fresh'	Z51 Kfs	Z51 Kfs
Wt.%									
MgO	0.03	0.00	0.02	0.00	0.00	0.01	0.09	0.00	0.26
Al_2O_3	20.85	20.18	21.16	20.26	19.66	19.57	29.30	18.60	17.78
SiO_2	67.67	67.99	66.70	69.26	69.28	69.00	53.63	65.85	66.05
CaO	0.76	0.51	1.66	0.78	0.26	0.35	11.79	0.00	0.16
FeO	0.11	0.05	0.12	0.31	0.42	0.08	0.85	0.17	0.34
K_2O	0.08	0.04	0.02	0.05	0.13	0.05	0.22	15.91	15.73
MnO	0.00	0.00	0.00	0.01	0.00	0.00	0.06	0.00	0.00
Na_2O	11.29	11.18	10.46	11.17	11.58	11.17	4.51	0.55	0.26
TiO_2	0.00	0.02	0.00	0.00	0.03	0.01	0.08	0.02	0.00
Total	100.79	99.99	100.14	101.84	100.25	100.25	100.52	101.10	100.59
Atoms per formula unit (8 O)									
Mg	0.00	0.00	0.00	0.00	0.01	0.00	0.01	0.00	0.02
Al	1.07	1.04	1.09	1.03	1.00	1.00	1.56	3.00	3.03
Si	2.94	2.97	2.92	2.97	2.99	2.99	2.42	1.00	0.96
Ca	0.04	0.02	0.08	0.04	0.02	0.01	0.57	0.00	0.01
Fe	0.00	0.00	0.00	0.01	0.01	0.02	0.03	0.01	0.01
K	0.00	0.00	0.00	0.00	0.01	0.01	0.01	0.93	0.92
Mn	0.00	0.00	0.00	0.00	0.00	0.00	0.00	0.00	0.00
Na	0.95	0.95	0.89	0.93	0.93	0.97	0.39	0.05	0.02
Ti	0.00	0.00	0.00	0.00	0.00	0.00	0.00	0.00	0.00
O	8.00	8.00	8.00	8.00	8.00	8.00	8.00	8.00	8.00
An	4.04	2.06	8.25	3.66	2.11	1.02	59.38		
Or								94.90	96.84

An – Anorthite; Or – Orthoclase

https://doi.org/10.1346/CCMN.2012.0600101 Published online by Cambridge University Press

morphic minerals such as: zeolites, chlorite/smectite, prehnite, pumpellyite, albite, epidote, quartz, and in some cases carbonates. In most of the samples, amygdales and fissures are filled with several types of secondary minerals. Stilbite, analcime, and heulandites present in the amygdales were replaced in many cases by laumontite, which in turn is replaced by prehnite and pumpellyite. Mafic phyllosilicates such as dioctahedral smectites change gradually to trioctahedral smectites, which in turn change to chlorite, with increasing metamorphic grade.

Zeolites. The presence of zeolites in the arc volcanics is well known from studies in other areas of the same arc (*e.g.* Bedelean, 1972; Istrate, 1980; Nicolae, 1994; Savu, 1996; Miron, 2006). Those studies identified stilbite, heulandite, mordenite, laumontite, chabazite, analcime, and epistilbite. Samples collected in the present study contain six zeolite types, all identified using XRD: heulandite, stilbite, analcime, laumontite, epistilbite, and mordenite (Table 1). Some of the zeolites from other outcrops were analyzed using EPMA. To ensure the quality of the microprobe data, the charge balance error, E, was calculated using $E = [(Al-Al_{theor})/Al_{theor}] \times 100$, where Al_{theor} = Na+K+2(Ca+Mg). Data linked with E >10% were discarded (Passaglia and Sheppard, 2001). In the case of mordenite, all E values were >10% and the analyses for this mineral were not considered further.

Analcime. This zeolite formed clusters, often together with heulandite, calcite, and albite ± quartz (Figure 2b). Several samples were analyzed by EPMA (Table 3). The composition of the tetrahedral network of analcime can be expressed by R (R = Si/(Si+Al)). The values of R in the samples analyzed were between 0.69 and 0.73 with an average value of 0.70. Extra-framework cations were dominated by Na, with the Na/(Na+K) ratio very close to 1 and the concentrations of Ca and Mg were <0.5 and <0.05 a.p.f.u., respectively.

Heulandite. Heulandite formed reddish-pink tabular crystals mainly in fissures (outcrop Z43), particularly in fissures and amygdales that also contain analcime (Z55 and Z57; Figure 2b) and partially replaced plagioclase in some samples (Figure 2a). The R values of samples analyzed in all three outcrops were between

Table 3. Representative compositions for analcime, laumontite, and heulandite determined by EPMA.

Outcrop	Z57 Anl	Z57 Anl	Z51 Lmt	Z44 Lmt	Z55 Hul	Z57 Hul	Z43 Hul
Wt.%							
MgO	0.02	0.01	0.64	0.04	0.11	0.01	0.08
Al_2O_3	21.65	21.09	18.90	22.27	16.82	18.10	19.46
SiO_2	58.30	56.35	47.31	54.19	63.97	61.33	58.12
CaO	0.03	0.03	9.51	11.73	8.41	8.91	9.93
FeO	0.01	0.01	0.95	0.06	0.35	0.11	0.13
K_2O	0.02	0.01	0.42	0.24	0.04	0.05	0.07
MnO	0.00	0.00	0.02	0.00	0.03	0.00	0.03
Na_2O	12.21	12.34	0.27	0.13	0.62	0.90	0.64
TiO_2	0.00	0.00	0.01	0.01	0.01	0.00	0.00
Total	92.23	89.85	78.04	88.67	90.36	89.41	88.47
Atoms per formula unit (96, 24, and 72 O)							
Mg	0.01	0.01	0.16	0.01	0.07	0.01	0.05
Al	14.69	14.73	3.80	3.92	8.51	9.30	10.18
Si	33.56	33.39	8.08	8.09	27.45	26.73	25.80
Ca	0.02	0.02	1.74	1.88	3.87	4.16	4.72
Fe	0.00	0.01	0.14	0.01	0.12	0.04	0.05
K	0.01	0.01	0.09	0.05	0.02	0.03	0.04
Mn	0.00	0.00	0.00	0.00	0.01	0.00	0.01
Na	13.63	14.17	0.09	0.04	0.52	0.76	0.55
Ti	0.00	0.00	0.00	0.00	0.00	0.00	0.00
O	96.00	96.00	24.00	24.00	72.00	72.00	72.00
R = Si/(Si+Al)	0.70	0.69	0.68	0.67	0.76	0.74	0.72
Na/(K+Na)	1.00	1.00	0.49	0.44	0.96	0.96	0.93
Ca/(Ca+Mg)	0.56	0.67	0.91	0.99	0.98	1.00	0.99
(Ca+Mg)/(Na+K)	0.002	0.002	0.095	0.044	0.14	0.19	0.12
2 × (Ca+Mg)+Na+K	13.70	14.25	3.99	3.86	8.42	9.12	10.15
E	7.19	3.41	-4.65	1.65	1.08	1.96	0.33

E = $[(Al-Al_{theor})/Al_{theor}] \times 100$ and Al_{theor} = Na+K+2(Ca+Mg)

https://doi.org/10.1346/CCMN.2012.0600101 Published online by Cambridge University Press

0.72 and 0.77, with an average of 0.75 (Table 3). Extra-framework cations include Ca, 3.93–4.72; Mg, 0–0.31; Na, 0.24–1.20; and K, 0.03–0.26 a.p.f.u.

Laumontite. Crystals were of mm scale, of prismatic habit, and milky color. Laumontite occurred in fissures as filling cement and also in amygdales together with other Ca silicates such as prehnite and pumpellyite (Figure 7a), and with albite, pumpellyite, and C/S (Figure 6c). Laumontite had *R* values between 0.66 and 0.68 with an average of 0.68. Extra-framework cations include: Ca, 1.74–1.98; Mg <0.05; Na <0.18; and K <0.10 a.p.f.u.

Other zeolites. Mordenite, epistilbite, and stilbite were identified by XRD only. Mordenite was present only in amygdales along with epistilbite and had a white–pink color. Epistilbite formed pink-reddish clusters. Stilbite occurred in fissures, together with laumontite and occurred with mordenite and with heulandite in amygdales (Z43). Stilbite and stellerite often form a solid solution (Fridriksson *et al.*, 2001). Because of their similar structures, the XRD patterns of the two zeolites are almost identical. Distinguishing between the two is challenging, except at 23–25°2θ, where two distinct peaks are discernible in the case of stilbite (for 204 and $20\bar{4}$ reticular planes) due to its monoclinic crystal structure. In the case of stellerite which has an orthorhombic crystal structure, the peak corresponding to the $20\bar{4}$ reticular plane is missing. Peaks in the 23–25°2θ area suggest that stellerite could have been present, particularly in the case of the sample from outcrop Z55, where the peak for the $20\bar{4}$ reticular plane had the lowest intensity (Figure 3).

Mafic phyllosilicates. Mafic phyllosilicates were ubiquitous secondary minerals throughout the outcrops sampled; they replaced primary silicate minerals (Figure 2a) and were often found in the groundmass, in fissures, and in amygdales. In some cases phyllosilicates were the only minerals infilling amygdales. In outcrop Z43, mafic phyllosilicates were present in two amygdale types: one with heulandite at the rim and C/S filling the interior, and another with dioctahedral and trioctahedral smectite at the rim and C/S and mordenite in the interior, filling most of the volume (Figure 6a,b). In most cases they occurred together with zeolites such as mordenite, heulandite, and laumontite and other minerals such as albite, prehnite, pumpellyite, calcite, quartz, and epidote (Figure 6). Under the optical microscope, two types of phyllosilicates could be discerned. In plane polarized light, one type had a brown-orange color and the other type was yellowish-green. The former had a moderately high birefringence and was typically masked by strong body colors, and the latter had lower birefringence. The EPMA results revealed that the optical properties for the first type are characteristic of greater smectite content.

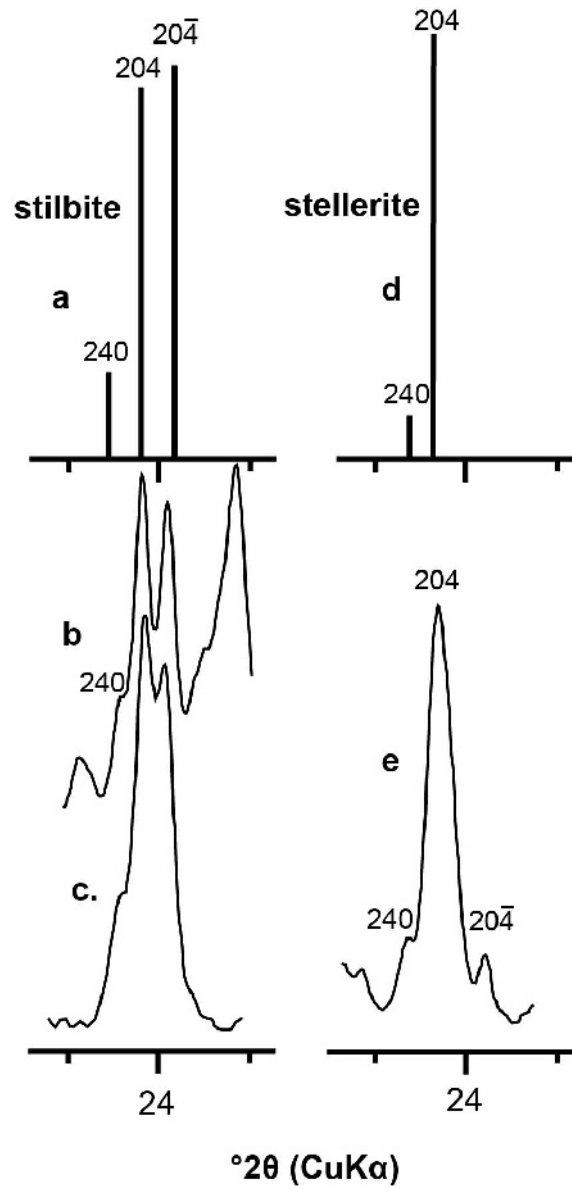

Figure 3. XRD patterns (23–25°2θ area) for stilbite and stellerite. XRD peak positions and relative intensities of stilbite (a) and stellerite (d) are as by Treacy *et al.* (2001). (b) Sample from outcrop Z43. (c) Sample from outcrop Z57. (e) Sample from outcrop Z55.

For the second type, optical properties were typical of higher chlorite content.

The chemical composition of mafic phyllosilicates was analyzed from several samples and outcrops (Table 4, Figure 4). Some samples had an intermediate composition between dioctahedral and trioctahedral smectite (particularly those from outcrops Z43, Z55, and Z57). These were samples which had a molar sum of Si+Al+Mg+Fe <17.82 and >2 wt.% CaO. The majority of the samples had an intermediate composition between trioctahedral smectites

https://doi.org/10.1346/CCMN.2012.0600101 Published online by Cambridge University Press

Table 4. Representative compositions for mafic phyllosilicates determined by EPMA.

Outcrop	Z43 C/S	Z43 Di-tri smectite	Z43	Z44	Z51	Z51	Z52 C/S	Z55	Z55	Z57
Wt.%										
MgO	13.36	11.11	9.40	15.56	19.65	18.79	17.13	12.77	14.21	10.68
Al_2O_3	12.64	16.33	14.85	15.61	19.85	14.51	16.62	12.19	13.09	11.24
SiO_2	37.73	42.09	43.10	31.27	30.48	35.82	30.15	36.17	31.02	29.48
CaO	1.00	2.67	3.56	0.55	0.30	0.84	0.31	1.33	0.62	0.26
FeO	20.45	13.45	14.49	20.68	15.05	12.34	18.70	20.74	23.26	33.05
K_2O	0.29	0.47	0.29	0.06	0.01	0.12	0.05	0.17	0.05	0.08
MnO	0.09	0.05	0.09	0.56	0.17	0.14	0.35	0.24	0.43	0.60
Na_2O	0.60	0.61	0.51	0.33	0.11	0.28	0.12	0.30	0.04	0.10
TiO_2	0.02	0.01	0.01	0.00	0.00	0.00	0.00	0.00	0.02	0.00
Total	86.19	86.78	86.31	84.62	85.62	82.83	83.43	83.91	82.73	85.48
Atoms per formula unit (28 O)										
Mg	4.08	3.21	2.74	4.92	5.92	5.73	5.43	4.03	4.67	3.61
^{IV}Al	0.28	3.73	3.42	1.37	1.84	0.68	1.59	0.35	1.16	1.31
^{VI}Al	2.77			2.53	2.89	2.82	2.58	2.70	2.25	1.70
Si	7.72	8.15	8.43	6.63	6.16	7.32	6.41	7.65	6.84	6.69
Ca	0.22	0.55	0.75	0.13	0.07	0.18	0.07	0.30	0.15	0.06
Fe(II)	3.50	2.18	2.37	3.67	2.54	2.11	3.33	3.67	4.29	6.27
K	0.08	0.12	0.07	0.02	0.00	0.03	0.01	0.04	0.01	0.02
Mn	0.02	0.01	0.01	0.10	0.03	0.02	0.06	0.04	0.08	0.12
Na	0.24	0.23	0.19	0.14	0.04	0.11	0.05	0.12	0.02	0.04
Ti	0.00	0.00	0.00	0.00	0.00	0.00	0.00	0.00	0.00	0.00
O	28.00	28.00	28.00	28.00	28.00	28.00	28.00	28.00	28.00	28.00
Si+Al+Mg+Fe	18.35	17.25	16.96	19.12	19.36	18.65	19.34	18.40	19.21	19.59
2*Ca+Na+K	0.75	1.45	1.76	0.40	0.17	0.51	0.20	0.77	0.33	0.19
Fe/(Fe+Mg) mol	0.40	0.40	0.46	0.43	0.30	0.26	0.38	0.51	0.48	0.63
MgO/(MgO+FeO)	0.40	0.45	0.39	0.43	0.57	0.60	0.48	0.38	0.38	0.24
Si/(Si+Al)	0.72	0.69	0.71	0.63	0.57	0.68	0.61	0.72	0.67	0.69
% Chlorite	24.42	–	–	59.47	70.51	38.17	69.60	26.45	63.70	81.21

and chlorite, mixed-layer chlorite/smectite (Figure 4). The term "mixed-layer chlorite/smectite" was used here without reference to layer ordering (Reynolds, 1988), which was not determined for these samples.

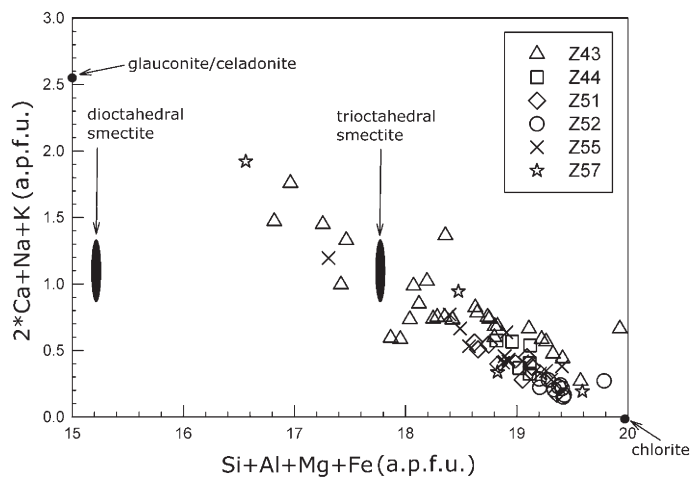

Figure 4. Composition of mafic phyllosilicates in basalts from the Balşa-Techereu-Poieniţa area, normalized to 28 oxide charge equivalents. The total moles of charge of exchangeable cations ($2 \times Ca+Na+K$) are plotted as a function of the total molar (Si+Al+Mg+Fe) content. Ideal end-member compositions of chlorite, celadonite (filled circles), trioctahedral smectite, and dioctahedral smectite (filled ovals) are also depicted.

https://doi.org/10.1346/CCMN.2012.0600101 Published online by Cambridge University Press

The increase in the amount of chlorite was accompanied by a decrease in the amount of Si, in agreement with the smaller Si content of the chlorite crystal lattice compared to smectite, although chlorite has a greater proportion of non-interlayer cations (Figure 5).

The compositional variability of mafic phyllosilicates was high within the sample sets and among outcrops. The Fe/(Fe+Mg) ratio for phyllosilicates varied from 0.45 to 0.51 for samples from outcrop Z55, from 0.42 to 0.49 for samples from outcrops Z43 and Z44, and from 0.30 to 0.38 in samples from outcrops Z51 and Z52. The percentage of chlorite was highest in outcrop Z52, with values ranging from 63 to 90% (σ 7.53) (σ representing the standard deviation). In outcrops Z44 and Z51, chlorite in C/S had values of 45−60% (σ 5.54) and of 36−70% (σ 12.01), respectively. In these outcrops, C/S filled amygdales together with albite, prehnite, and pumpellyite (Figure 6c). Outcrop Z43 showed a large range of chlorite abundance in C/S, from 6 to 96% (σ 25.41). The range for Z55 was smaller, with values of 26−72% (σ 14.41). An increase in chlorite percentage was observed from the rim to the center of the amygdales.

The mafic phyllosilicates from outcrop Z57 had an Al content <11.24 wt.%. The Fe/(Fe+Mg) molar ratio measured between 0.60 and 0.63. Samples from Z57 also had >29 wt.% FeO and an Fe/(Fe+Mg) ratio >0.5. All other outcrops had FeO $\leqslant$20 wt.% (Table 3) and Fe/(Fe+Mg) ratio $\leqslant$0.5.

Glauconite. In outcrop Z57, K was a dominant interlayer cation in some of the phyllosilicates, with K $\approx$ 6 wt.% (Table 5). This may indicate the presence of glauconite or celadonite. Using the IMA classification (International Mineralogical Association, Rieder *et al.*, 1998) the two samples analyzed fall in the glauconite field, with an interlayer charge between 0.6 and 0.8 (glauconite 0.6−0.85). The samples had a tetrahedral sheet occupancy >2 a.p.f.u., which is the ideal occupancy for dioctahedral clays. This occupancy can be explained by the presence of a trioctahedral clay mineral associated with glauconite.

Pumpellyite. In samples from Z44, pumpellyite was present as a fine granular mass in the matrix and as radiating granules in the amygdales. Under the optical microscope, the mineral was slightly green/yellow to brown and had anomalous interference colors. Pumpellyite was associated with secondary albite, laumontite, prehnite, and rarely with C/S (Figure 6c). From its textural appearance, laumontite seemed to be replaced by prehnite and pumpellyite (Figure 7a). In outcrop Z51, pumpellyite occurred in amygdales with albite or C/S or, in some amygdales, with both, and as fine crystals replacing plagioclase feldspar (Figure 7b). Under the optical microscope, the pumpellyite replacing plagioclase showed no pleochroism and had anomalous interference colors. Pumpellyite present in amygdales had a slightly greenish color.

Pumpellyite chemical compositions differed somewhat from outcrop to outcrop (Table 5; note that all Fe was considered to be Fe(II)). In the case of Z51, the X_{Mg}, calculated as Mg/(Mg+Fe), was >0.3 with an average value of 0.47, whereas in outcrop Z44, X_{Mg} was <0.3 and had an average value of 0.22. Pumpellyites in Z44 contained more Fe, with a total FeO of 9.20−16.19 wt.%, and an average of 13.58 wt.%. In outcrop Z51, FeO was between 2.92 and 11.64 wt.%, with an average of 5.54 wt.%. The Mg to Fe ratio average value was 1.14 for Z51 and 0.29 for Z44. The X_{Fe}, calculated as the ratio Fe/(Fe+Al), had an average value of 0.15 for outcrop Z51 pumpellyites and 0.36 for Z44 pumpellyites.

In the case of Z51, pumpellyite that replaced plagioclase had an Fe content of 2.92−3.94 wt.% and X_{Fe} between 0.08 and 0.10. Amygdalar pumpellyite

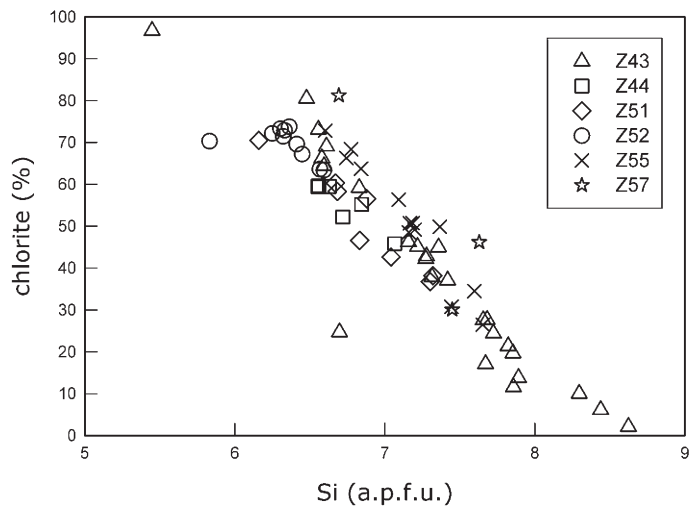

Figure 5. The percentage of chlorite *vs.* Si (a.p.f.u.) for C/S-type mafic phyllosilicates from the outcrops studied.

https://doi.org/10.1346/CCMN.2012.0600101 Published online by Cambridge University Press

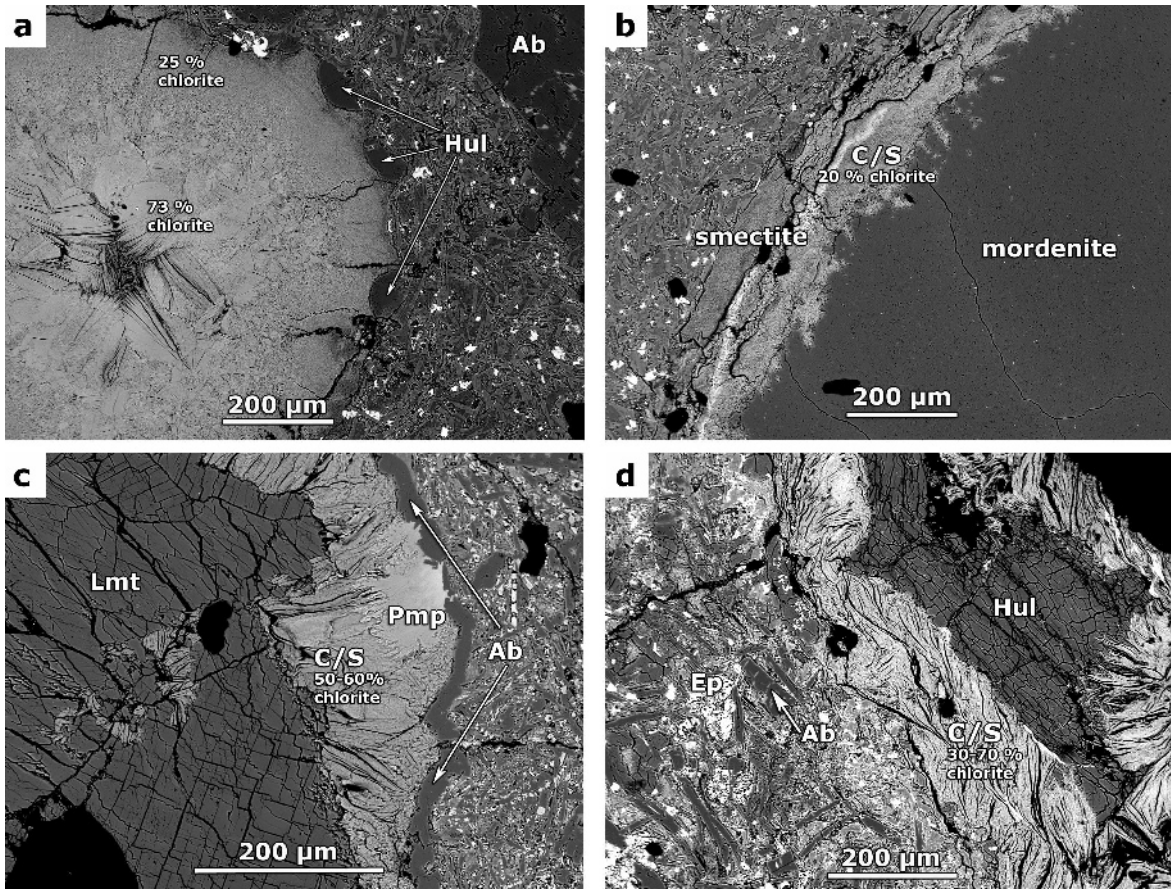

Figure 6. BSE images. (a) Amygdale filled with heulandite (Hul) and C/S (Z43). (b) Amygdale filled with smectite, C/S, and mordenite (Z43). (c) Amygdale filled with secondary albite (Ab), pumpellyite (Pmp), C/S, and laumontite (Lmt) (Z44). (d) Amygdale filled with C/S and heulandite (Hul), in matrix of epidote (Ep) and albite (Ab) (Z55).

present in association with albite or C/S had Fe content of 8.60−11.64 wt.% and X_{Fe} between 0.23 and 0.32, similar to the pumpellyites from Z44 (Figure 8). The Mg content in both pumpellyites was nearly identical, with values from 2.32 to 3.00 wt.% for the first type and 2.51 and 2.88 wt.% for the second type.

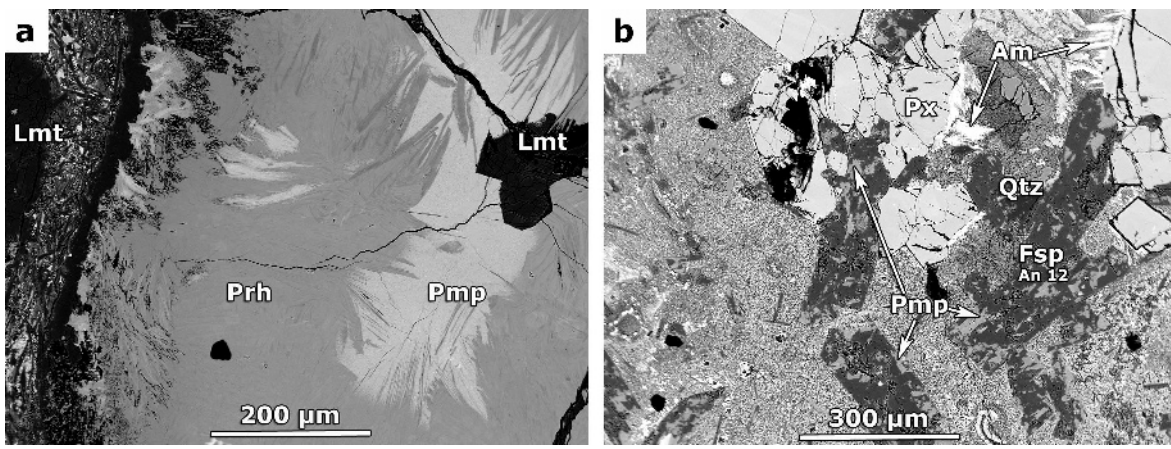

Figure 7. BSE images. (a) Amygdale filled with prehnite (Prh), pumpellyite (Pmp), and laumontite (Lmt) (Z44). (b) Pumpellyite replacing partially albitized plagioclase and amphibole (Am) needles growing from the pyroxene (Px) (Z51).

https://doi.org/10.1346/CCMN.2012.0600101 Published online by Cambridge University Press

Table 5. Representative compositions for pumpellyite and secondary amphibole determined by EPMA.

Outcrop	Z51 Pmp	Z51 Pmp	Z44 Pmp	Z44 Pmp	Z51 Am	Z51 Am	Z43 Am
Wt.%							
MgO	2.63	2.51	2.10	2.10	11.43	9.97	14.45
Al_2O_3	25.27	17.24	20.73	16.79	2.44	6.94	2.00
SiO_2	38.16	36.88	37.31	37.01	54.07	50.71	52.93
CaO	22.94	22.40	22.36	21.90	12.51	13.50	10.99
FeO	3.12	11.64	9.20	14.01	16.67	10.67	10.97
K_2O	0.00	0.00	0.02	0.01	0.07	0.06	0.04
MnO	0.00	0.10	0.22	0.16	0.72	0.63	0.33
Na_2O	0.05	0.01	0.07	0.05	0.19	1.17	0.25
TiO_2	0.05	0.06	0.02	0.05	0.00	0.79	0.04
Total	92.22	90.84	92.03	92.08	98.1	94.43	92.01
Atoms per formula unit (24.5 and 23 O)							
Mg	0.63	0.65	0.52	0.54	2.49	2.21	3.25
Al	4.79	3.51	4.09	3.41	0.42	1.21	0.36
Si	6.14	6.37	6.25	6.37	7.89	7.53	7.98
Ca	3.95	4.14	4.01	4.04	1.96	2.15	1.78
Fe	0.42	1.68	1.29	2.02	2.03	1.33	1.38
K	0.00	0.00	0.01	0.00	0.01	0.01	0.01
Mn	0.00	0.01	0.03	0.02	0.09	0.08	0.04
Na	0.02	0.00	0.02	0.02	0.05	0.34	0.07
Ti	0.01	0.01	0.00	0.01	0.00	0.09	0.00
O	24.50	24.50	24.50	24.50	23.00	23.00	23.00
X_{Mg}	0.60	0.28	0.29	0.21	0.55	0.62	0.70
MgO/(MgO+FeO)	0.46	0.18	0.19	0.13	0.41	0.48	0.57
X_{Fe}	0.08	0.32	0.24	0.37	0.83	0.52	0.80
Mg/Fe	1.50	0.38	0.41	0.27	1.22	1.67	2.35
AF	-121.47	-139.18	-116.99	-109.21	-39.57	-45.42	-34.35

$AF = 100 \times (Al_2O_3+Fe_2O_3-0.75 \times CaO-Na_2O+0.75 \times TiO_2)/(Al_2O_3+Fe_2O_3-0.75 \times CaO-Na_2O+0.75 \times TiO_2+ FeO+MgO)$
All analyses were recalculated on the basis of a pumpellyite formula with 24.5 O and an amphibole formula with 23 O. All Fe was considered to be Fe(II).

For Z44, MgO/(FeO+MgO) values were between 0.10 and 0.19 for matrix pumpellyites, whereas Z51 values were at 0.18 and 0.23 for amygdalar pumpellyites and at 0.40 to 0.50 for plagioclase feldspar replacing pumpellyite.

Prehnite. Prehnite was present in several samples together with pumpellyite. In outcrop Z44 it was present in amygdales together with albite, laumontite, pumpellyite, and C/S. It was also present in considerable amounts in the matrix. Under the optical microscope, prehnite was colorless with low relief and formed irregular patches. In some cases the prehnite had a pale brown color, probably due to the presence of Fe in the crystal lattice. Amygdale textural relations suggest that prehnite replaced laumontite together with pumpellyite and C/S (Figure 7a). In outcrop Z51, prehnite occurred in amygdales together with albite and quartz. Also present in the sample were amygdales with pumpellyite, C/S, and albite, or with epidote, albite, C/S, and quartz. Amygdales were observed with rims of euhedral albite crystals, filled with colorless, low-relief, high-birefringence prehnite crystals.

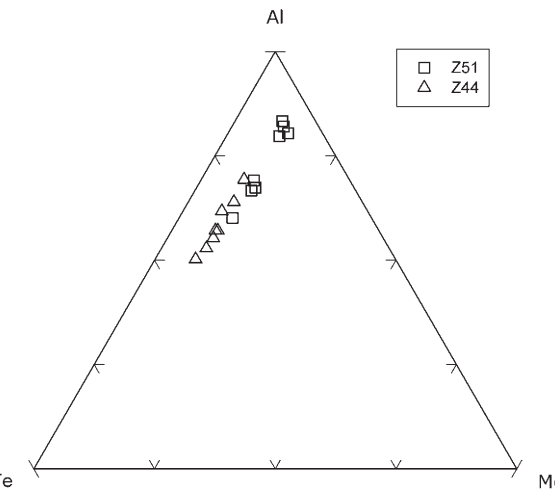

Figure 8. Pumpellyite compositions in terms of Al-Fe-Mg. All analyses were recalculated on the basis of a pumpellyite formula with 24.5 O and all Fe was considered to be Fe(II).

https://doi.org/10.1346/CCMN.2012.0600101 Published online by Cambridge University Press

Prehnite crystals had variable Fe concentration, between 0.83 and 2.33 wt.% in Z51 and between 0.05 and 6.60 wt.% in Z44 (Table 6). The X_{Fe}, calculated as the ratio Fe/(Fe+Al), ranged between 0 and 0.18.

Epidote. Epidote occurred in most of the outcrops and samples studied, usually as xenomorphic to idiomorphic grains in plagioclase, in veins and amygdales, and most often in the matrix. Epidote was identified under the optical microscope in the following outcrops: Z43 in the matrix associated with calcite and C/S. In these samples, stilbite fissures, calcite late fissures, amygdales filled with C/S cut by heulandite fissures, and amygdales filled with C/S and mordenite were present. In Z55 and Z53, epidote was observed in the matrix associated with heulandite, C/S (Figure 6d), and stilbite. In these outcrops, fissures with laumontite + calcite were identified. In Z47 epidote was found in the matrix together with C/S. In Z54, epidote was present in the amygdales with calcite, C/S, and epistilbite. In Z51, epidote was present in amygdales together with quartz ± pumpellyite/prehnite, and also in amygdales with C/S, albite, and quartz. In this outcrop, prehnite + quartz amygdales were also identified. No pumpellyite or prehnite were present in outcrop Z52. In this outcrop, epidote was found in amygdales along with calcite and quartz and was also found in feldspars along with calcite.

Epidote from outcrops Z51 and Z52 was analyzed chemically and optically (Table 6). Chemical compositions showed no significant variation, with average Fe contents of 9.12 and 9.03 wt.% Fe_2O_3, respectively (all Fe was considered to be Fe(III)). The X_{Fe} values were also similar, with an average value of 0.18 in samples from both outcrops.

Amphibole. Amphibole was found only in samples from outcrop Z51. Under the optical microscope it usually appeared as green, acicular grains radiating from primary pyroxene. Amphibole was also seen in the matrix as very fine grains together with C/S, pumpellyite ± prehnite, albite, and epidote. From chemical analysis it appeared to be calcic, with similar proportions of Ca and Fe. The Al content varied between 2 and 7 wt.% and the calculated MgO/(MgO+FeO) ratios were from 0.55 to 0.70 (Table 5).

DISCUSSION

Chlorite/smectite mixed layering

Reactions are generally slow in low-temperature environments, and phyllosilicates usually do not achieve equilibrium. Important information regarding the degree of disequilibrium and reaction progress can be gleaned, however, from the compositions and compositional

Table 6. Representative compositions for prehnite and epidote determined by EPMA.

Outcrop	Z51 Prh	Z51 Prh	Z44 Prh	Z44 Prh	Z52 Ep	Z52 Ep	Z51 Ep	Z51 Ep
Wt.%								
MgO	0.04	0.03	0.05	0.03	0.05	0.08	0.11	0.19
Al_2O_3	21.42	22.22	18.87	19.97	26.70	24.40	23.82	25.06
SiO_2	42.88	44.00	43.33	43.02	39.23	38.78	38.80	39.20
CaO	26.72	26.95	26.02	26.15	23.38	23.15	23.64	23.66
Fe_2O_3	1.88	1.18	6.60	3.84	8.18	10.46	10.03	8.98
K_2O	0.06	0.01	0.01	0.00	0.00	0.02	0.00	0.01
MnO	0.12	0.00	0.04	0.06	0.26	0.20	0.14	0.15
Na_2O	0.12	0.06	0.06	0.08	0.00	0.01	0.02	0.01
TiO_2	0.04	0.14	0.00	0.00	0.11	0.08	0.02	0.08
Total	93.28	94.58	94.98	93.17	97.92	97.17	96.58	97.34
Atoms per formula unit (11 and 12.5 O)								
Mg	0.00	0.00	0.01	0.00	0.01	0.01	0.01	0.02
Al	1.79	1.83	1.57	1.68	2.45	2.28	2.24	2.33
Si	3.05	3.07	3.06	3.08	3.06	3.07	3.10	3.09
Ca	2.04	2.01	1.97	2.00	1.95	1.97	2.02	2.00
Fe^{3+}	0.10	0.06	0.35	0.21	0.48	0.62	0.60	0.53
K	0.01	0.00	0.00	0.00	0.00	0.00	0.00	0.00
Mn	0.01	0.00	0.00	0.00	0.02	0.01	0.01	0.01
Na	0.02	0.01	0.01	0.01	0.00	0.00	0.00	0.00
Ti	0.00	0.01	0.00	0.00	0.01	0.00	0.00	0.00
O	11.00	11.00	11.00	11.00	12.5	12.5	12.5	12.5
X_{Fe}	0.05	0.03	0.18	0.11	0.16	0.21	0.21	0.19

All Fe was considered to be Fe(III).

https://doi.org/10.1346/CCMN.2012.0600101 Published online by Cambridge University Press

variation in secondary mineral assemblages. One characteristic parameter of C/S-type phyllosilicates is the chlorite percentage, which is known to increase with increasing temperature, but can also be influenced by other factors (Schiffman and Fridleifsson, 1991; Robinson and Bevins, 1994). The data set showed a wide range of chlorite contents in C/S, a feature that could be attributed to the slow reaction kinetics involving phyllosilicates. Values differ not only between outcrops, but also from sample-to-sample within the same outcrop. In outcrops Z43, Z55, and Z57, the percentage of chlorite displays significant variability (*e.g.* 6−96%, with σ 25.4 in outcrop Z43). In outcrops Z44 and Z52, the variation is smaller (45−60% and 63−90%, respectively, with σ 5.5−7.5). In the case of grains with large amounts of Ca (>2 wt.%), the presence of discrete smectite was considered, as fine grains, as this amount of Ca (+ Na and K) is probably not hosted in the smectite layers of the C/S alone (Miyahara *et al.*, 2005). The difference between outcrops Z44 and Z52 and the other outcrops that have larger ranges of values could be due to a difference in fluid/rock ratios. Outcrops Z43, Z55, and Z57 are pyroclastic and, therefore, are likely to have had greater porosity than the basaltic andesite lava flows that make up outcrops Z44 and Z52. A low integrated fluid/rock ratio would restrict the supply of nutrients, thus acting as a kinetic constraint on the smectite-to-chlorite transition, resulting in a wide range of values for the chlorite content (Schiffman and Staudigel, 1995). In contrast, a relatively high fluid/rock ratio would favor the crystallization of discrete chlorite (Schiffman and Staudigel, 1995).

The importance of chemical components available was illustrated *via* a very good correlation of chlorite variation in C/S with feldspar albitization, as C/S was formed by alteration of volcanic glass and primary minerals such as feldspars (Alt, 1999; Giorgetti *et al.*, 2006, 2009). Samples with relict feldspars or little albitization had the greatest variation in chlorite percentage, with continuous smectite to chlorite throughout C/S mixed layering (*e.g.* Z43 feldspars had An >50 and 6−96% of chlorite in C/S, σ 25.4; Z51 had mostly albitized plagioclase plus relict plagioclase of An_{50}, with 37−70% of chlorite in C/S, σ 12). Outcrops where all feldspars were completely replaced, with <3% An, had the smallest variability in chlorite percentage (*e.g.* samples from outcrop Z44 had 45−60% chlorite, σ 5.5; samples from Z52 had 63−90% chlorite, σ 7.5, with discrete chlorite), suggesting that Al availability was not a limiting factor governing the composition of these samples.

Similar phyllosilicates have been described from basaltic lava flows in west Greenland (Neuhoff *et al.*, 2006) where mafic phyllosilicate compositions become systematically richer in the trioctahedral component with increasing depth (and increasing temperature). Drief and Schiffman (2004) suggest either the possibility of a mechanical mixture of discrete phases or an interstratification of di- and trioctahedral clay. The increase in chlorite content often signifies an increase in temperature (Schiffman and Fridleifsson, 1991) but high chlorite content can also be related to feldspar alteration, which releases the Al needed to form chlorite (Shau and Peacor, 1992; Schmidt and Robinson, 1997). The general increase in chlorite content in the C/S, from amygdale rims to the center, is related to an increase in temperature. However, local chlorite variability is limited by reaction kinetics, which are controlled by the availability of necessary elements such as Al (Schiffman and Fridleifsson, 1991; Shau and Peacor, 1992; Schmidt and Robinson, 1997; Neuhoff *et al.*, 2006).

Epidote projections

The paragenetic relations of pumpellyite and chlorite grains in physical contact were examined in the NCFMASH system *via* the epidote projection (Beiersdorfer, 1993). The epidote projection is constructed in terms of an eight-component system, SiO_2-(Al_2O_3+Fe_2O_3)-FeO-MgO-CaO-Na_2O-TiO_2-H_2O. Fe_2O_3 and Al_2O_3 are combined as a single component and, because of this, the $AlFe_{-1}$ type substitution is not considered. The system is suitable for expressing most of the low-*T* metamorphic mineral assemblages (Beiersdorfer, 1993). The projection was made by reducing the eight-component system using AF expression. The samples were plotted onto an AF-MgO/(MgO+FeO) plane, where relations between coexisting minerals, in this case pumpellyite and chlorite, may be shown (Figure 9). In all samples considered, quartz, albite, C/S (with chlorite >60%), epidote, and pumpellyite ± prehnite were present. Such assemblages are indicative of an H_2O fluid phase with very low X_{CO_2} (Digel and Ghent, 1994). To construct the projection, phases such as albite, quartz, and H_2O were considered to be in excess. All Fe in pumpellyite was considered to be Fe(II), as the estimation of Fe(III) does not have a significant effect on the mineral projection (Beiersdorfer, 1993) and an imperfect estimate would generate distortion (Bevins and Robinson, 1995).

The majority of the coexisting mineral pairs showed near parallel tielines and had relatively large spreads of compositions for both chlorite/smectite and pumpellyite (Figure 9). A surprising degree of consistency existed, considering the presence of chlorite/smectite mixed layering and the possibility of distortion due to smectite. The fact that the pumpellyite-chlorite/smectite tielines were parallel both in the case of different samples and different outcrops could indicate that the same metamorphic event generated all the observed assemblages, assuming equilibrium or near equilibrium for mineral pairs (minerals in physical contact). As equilibrium is impossible to prove, a test for disequilibrium would involve partitioning of Fe and Mg between pumpellyite

https://doi.org/10.1346/CCMN.2012.0600101 Published online by Cambridge University Press

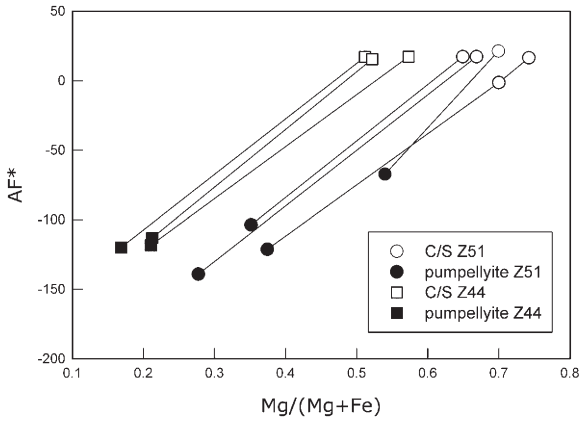

Figure 9. Epidote projection for C/S and pumpellyite pairs from outcrops Z51 and Z44. AF = $100 \times (Al_2O_3+Fe_2O_3-0.75 \times CaO-Na_2O+0.75 \times TiO_2)/(Al_2O_3+Fe_2O_3-0.75 \times CaO-Na_2O+0.75 \times TiO_2+FeO+MgO)$, with all values in molecular proportions. All Fe in pumpellyite is taken as Fe(II).

and chlorite mineral pairs, represented by K_d (Fe/Mg in pumpellyites over Fe/Mg in C/S). In the case of Z51, values were between 0.14 and 0.29 for the tielines of pumpellyites–chlorites with one exception (0.5 for the tieline that crossed the parallel ones). These data show that most of the mineral pairs were close to equilibrium and some show disequilibrium. In the case of Z44, the K_d values have less variation and ranged from 0.18 to 0.26, suggesting near-equilibrium at the sample scale. These values were comparable to those of pairs from outcrop Z51. Thus, from the partitioning factor, K_d, the assumption can be made that the samples were close to equilibrium and that disequilibrium occurred in the case of the intersecting tieline.

The range in composition for pumpellyite and chlorite/smectite in samples analyzed was probably due to a difference in bulk composition and relatively slow homogenization kinetics in these minerals. In the case of the intersecting tielines, the minerals were probably not equilibrated with respect to the other samples (local equilibrium), or they do not represent equilibrium pairs (Springer *et al.*, 1992).

Mineral assemblages and metamorphic facies

The minerals observed in each sample were assigned to one of two main assemblages (1 or 2) of distinct metamorphic grade.

The lowest-temperature assemblage was the one in which glauconite occurred together with heulandite + analcime + quartz, high Fe C/S, and discrete dioctahedral smectite. This mineral association was characteristic only of outcrop Z57 and was considered a subgroup of the next main assemblage. Mafic phyllosilicates from outcrop Z57 had high Fe/(Fe+Mg) values (>0.6) and a high FeO content (>29 wt.%). These features could be related to bulk-rock composition, but could also be influenced by the genetic conditions. When mixed-layer C/S was present, in particular, this ratio failed to correlate with bulk composition. Bevins *et al.* (1991a) noted that sedimentary chlorites have greater Fe contents, with Fe/(Fe+Mg) >0.5. Outcrops Z43, Z54, and Z55 were characterized by the main mineral assemblage (1) heulandite + analcime + quartz + C/S. Analcime was not present in samples where laumontite was present. It was probably converted to albite, which became more abundant. The R (R = Si/(Si+Al)) values for analcime were very similar to other low-temperature metamorphic analcimes reported in the literature (average R = 0.69, Passaglia and Sheppard, 2001). Laumontite was formed mainly as a result of feldspar albitization, which released the necessary elements. Analcime and stilbite were often precursor minerals of laumontite. Textural evidence showed that heulandite was partially replaced by analcime and that analcime was in turn replaced by albite with increasing temperature during dehydration reactions (Figure 2b). In the case of heulandite samples from outcrops Z55 and Z57, Na contents increased with decreasing Si, and Ca contents showed no correlation with Si. On the other hand, for heulandite samples from outcrop Z43, Ca contents increased with decreasing Si and Na contents were not correlated with Si (Si *vs.* Ca and Si *vs.* Na diagrams, Figure 10a,b). These two observations suggested that, in the crystal structure of heulandite, a Si-for-Na and Al-type substitution occurred in samples from outcrops Z55 and Z57, and a 2 × Si-for-Ca and 2 × Al-type substitution occurred in the case of samples from outcrop Z43. Both substitutions differ from the Na- and Si-for-Ca and Al plagioclase-type substitution. Zeolites often exhibit isomorphous substitutions between Si and Al in the tetrahedral framework and between charge-balancing extra-framework cations (Neuhoff and Ruhl, 2006, and others). One type of substitution is a coupled substitution of a single extra-framework cation (here, Na or Ca) with Al for Si, which is suggested to be a function of pressure, temperature, and the chemical potential of SiO_2 (Neuhoff and Ruhl, 2006). This phenomenon was also mentioned by Boak *et al.* (1991) and can be related to a sodic metasomatism that has been described in low-temperature metamorphic areas by Utada (1970), Coombs *et al.* (1976), and others, with fluids that are relatively rich in Na. This substitution appeared to be characteristic of samples from outcrops Z55 and Z57. In the case of samples from Z43, the fluids were probably more Ca rich, as analcime was not present, and the amygdale minerals showed an increase in Ca content, from heulandite on the rim followed by dioctahedral and trioctahedral smectites towards the interior. The C/S phyllosilicates associated with the above-described mineral assemblage showed a high compositional variability.

The second main mineral assemblage (2) found in the samples was laumontite + albite + quartz + prehnite-pumpellyite, and epidote. This assemblage was characteristic of outcrops Z44, Z50, and Z51, and is

https://doi.org/10.1346/CCMN.2012.0600101 Published online by Cambridge University Press

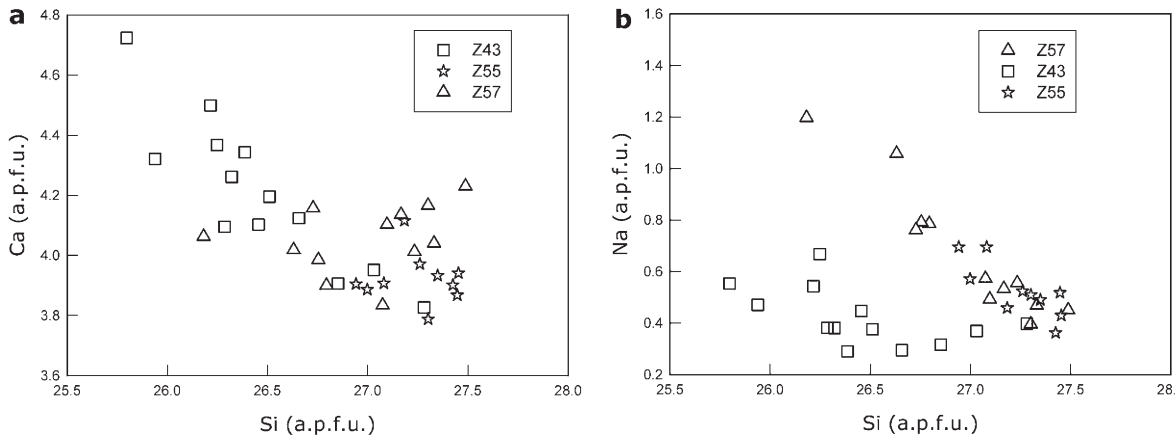

Figure 10. Ca *vs.* Si (a) and Na *vs.* Si (b) contents of heulandite, on the basis of a 72 oxygen framework.

associated with C/S phyllosilicates that have relatively large chlorite percentages and low variation in values.

In other outcrops, only epidote, chlorite, and calcite assemblages were found, with no prehnite-pumpellyite or other Ca-Al silicates (*e.g.* Z52). The high sensitivity of prehnite and pumpellyite (Liou *et al.*, 1987; Digel and Ghent, 1994) to CO_2 content of the metamorphic fluids (even at low CO_2 concentrations) could explain the fact that these minerals are absent in most of the samples where epidote is present together with calcite. Digel and Ghent (1994) used T-X_{CO_2} diagrams in the CMASH-CO_2 system to demonstrate that for prehnite and pumpellyite to be stable at temperatures up to 400ºC and pressures of 1.5 to 4.5 kbar, the mole fraction of CO_2 must be <0.002. At values >0.002, the assemblage epidote-chlorite-calcite assemblage stabilizes. Calcite found together with epidote could indicate local differences in fluid X_{CO_2} and calcite present in late veins could indicate a late, more CO_2-rich, fluid.

Extensive substitutions were identified for pumpellyite, pehnite, and epidote. The slight decrease in Mg and Al for relatively Fe-rich pumpellyites was probably due to $Fe^{2+}Mg_{-1}$ and $Fe^{3+}Al_{-1}$-type substitutions (Evarts and Schiffman, 1983, Maruyama and Liou, 1988). Such substitutions are typical of pumpellyites in low-temperature terrains (Bevins *et al.*, 1991a, 1991b), though only those present in low-variance buffered assemblages show real correlation between composition and metamorphism (Cho *et al.*, 1986). MgO/(FeO+MgO) values, for pumpellyites, were different from those in reports by Coombs *et al.* (1976) and Muñoz *et al.* (2010), where low values characterized pumpellyites present in plagioclase, contrary to the present case where lower values were characteristic of the pumpellyites in the matrix (0.10−0.19) and larger values for those present in the plagioclase (0.40−0.50). These differences were probably due to local bulk composition. Fe enrichment could also be attributed to relatively low temperatures and high oxygen fugacity (Liou, 1979; Evarts and Schiffman, 1983). In the case of prehnite and epidote, the principal compositional variation was due to an Fe(III)-for-Al substitution.

Prehnite probably stabilizes at temperatures of ~125ºC (Bevins *et al.*, 1991b). The association of laumontite with prehnite and pumpellyite clearly indicates transition between the upper zeolite facies and prehnite-pumpellyite facies. A rough estimate of temperature using Cathelineau's (1988) geothermometer yielded values of 164 to 220ºC. These values are generally consistent with the calcium silicate hydrous mineral assemblages. Temperature was calculated for C/S samples from Z51 with chlorite between 63 and 73% and is subject to error because of the presence of smectite (Essene and Peacor, 1995). The presence of amphibole together with the second main assemblage (2) is puzzling because amphibole is characteristic of the prehnite-pumpellyite, prehnite-actinolite, and pumpellyite-actinolite facies. Several authors have reported it from low-T metamorphic terrains, in subgreenschist metamorphic facies (Springer *et al.*, 1992; Beiersdorfer, 1993; Day and Springer, 2005). The MgO/(MgO+FeO) ratios in the C/S from outcrops where amphiboles were identified had the highest values, between 0.51 and 0.62. In all other outcrops where the ratio was lower, between 0.27 and 0.50, no amphibole could be identified. This could indicate a compositional control on the appearance of metamorphic amphibole (Robinson *et al.*, 2005; Bevins and Robinson, 1993; Beiresdorfer, 1993). The prehnite-pumpellyite facies is characterized by the presence of the two aforementioned minerals and the absence of zeolites. The presence of laumontite in the samples excludes the possibility of assigning the rocks to this facies.

All of the observations in the present study showed how the mineral assemblages and transition between metamorphic facies in low-temperature conditions are influenced by several factors starting with temperature, adding fluid characteristics (X_{CO_2}, fluid pressure–

https://doi.org/10.1346/CCMN.2012.0600101 Published online by Cambridge University Press

dehydration reactions, composition), and finishing with local bulk composition.

CONCLUSIONS

The presence of the minerals described above and their relations suggest that the rocks in the Balşa-Techereu-Poieniţa area were affected by low-temperature hydrothermal metamorphism. The nappe-stacking-related burial metamorphism can be excluded, as the lower tectonic unit (Feneş nappe) has seen only diagenetic to upper diagenetic-anchizone transition conditions (Ellero *et al.*, 2002). After Coombs (1960), the rocks could be included in the zeolite facies and could be separated into two phases: a lower-temperature phase with heulandite + analcime + quartz (*e.g.* samples from outcrop Z43), which formed at temperatures of <125ºC, and a higher-temperature phase with laumontite + albite + quartz + prehnite + pumpellyite ± amphibole (*e.g.* samples from outcrop Z51), which formed at temperatures up to 200ºC.

Outcrops Z44 and Z51 had minerals of higher-grade assemblages. These were part of the pyroclastite-containing sequence (Figure 1), where rocks had high porosity which would mean a high fluid/rock ratio which, in turn, determined somewhat higher alteration and rather fast mineral reactions, resulting in low mineral variations, especially in terms of the amount of chlorite in C/S. Another possibility is that these rocks were situated much closer to the hydrothermal vent system of the volcanic islands (heat flow from the volcanic activity), and thus were affected by higher-temperature fluids. On the other side, the outcrops that showed a relatively lower grade and greater variability in terms of chlorite content (*e.g.* Z43, Z55, and Z57) were part of the sequence consisting mainly of lava flows (Figure 1), which had somewhat lower porosity, leading to a rather small fluid/rock ratio and slow mineral reactions.

An increasing metamorphic grade was suggested by the increasing amount of chlorite in C/S from the rim to the center of the amygdales. Depending on particular conditions such as fluid/rock ratio (*i.e.* variation in the amount of chlorite was correlated with alteration of feldspars in lava flows and pyroclasts, due to differences in fluid-rock ratio), local chemistry (*i.e.* the stability of amphibole only in samples where MgO/(FeO+MgO) is >0.51), and fluid chemistry (*i.e.* mineral sequences in amygdales and the absence of prehnite and pumpellyite due to CO_2-rich fluids), differences in the mineral assemblage were common and no clear metamorphic-facies transition was present.

ACKNOWLEDGMENTS

The present research was made possible by financial support from the Scientific Performance Scholarship awarded by Babeş Bolyai University, Cluj-Napoca, and the Central European Exchange Program for University Studies. The authors thank Dr Dan Topa and Dr Ferenc Kristály for assisting with analytical work. G.D.M. thanks Prof. Dr Christoph A. Heinrich and Dr Eng. Lucian-Cristian Pop for fruitful discussions and a preliminary review, and the other reviewers for their comments which helped to improve the manuscript.

REFERENCES

Alt, J.C. (1999) Very low-grade hydrothermal metamorphism of basic igneous rocks. Pp. 169–201 in*:* *Low-grade Metamorphism* (M. Frey and M. Robinson, editors). Blackwell Science, Oxford, UK.

Árkai, P., Mata, M.P., Giorgetti, G., Peacor, D.R., and Toth, M. (2000) Comparison of diagenetic and low-grade metamorphic evolution of chlorite in associated metapelites and metabasites: an integrated TEM and XRD study. *Journal of Metamorphic Geology*, **18**, 531–550.

Bedelean, I. (1972) Zeoliţii din Munţii Apuseni şi fenomenul de zeolitizare. PhD Thesis, University of Babeş-Bolyai, Cluj-Napoca, Romania.

Beiersdorfer, R.E. (1993) Metamorphism of a Late Jurassic volcano-plutonic arc, northern California, U.S.A. *Journal of Metamorphic Geology*, **11**, 415–428.

Bettison, V., Mackinnon, J.D.R., and Schiffman, P. (1991) Integrated TEM, XRD and electron microprobe investigation of mixed-layer chlorite-smectite from the Point Sal ophiolite, California. *Journal of Metamorphic Geology*, **9**, 697–710.

Bevins, R.E. and Robinson, D. (1993) Parageneses of Ordovician sub-greenschist to greenschist facies metabasites from Wales, UK. *European Journal of Mineralogy*, **5**, 925–935.

Bevins, R.E. and Robinson, D. (1995) Regional low-grade polygenetic metamorphism and inversion in the northern part of Eastern Belt, northern Sierra Nevada, California. Pp. 29–50 in: *Low-Grade Metamorphism of Mafic Rocks* (P. Schiffman and H.W. Day, editors). Geological Society of America Special Paper, **296**.

Bevins, R.E., Robinson, D., and Rowbotham, G. (1991a) Compositional variation in mafic phyllosilicates from regional low grade metabasites and their application of the chlorite geothermometer. *Journal of Metamorphic Geology*, **9**, 711–721.

Bevins, R.E., Rowbotham, G., and Robinson, D. (1991b) Zeolite to prehnite-pumpellyite facies metamorphism of the late Proterozoic Zig-Zag Dal Basalt Formation, eastern North Greenland. *Lithos*, **27**, 155–165.

Boak, J.M., Cloke, P., and Broxton, D. (1991) Mineral chemistry of clinoptilolite and heulandite in diagenetically altered tuffs from Yucca Mountain, Nye County, Nevada. *Geological Society of America, Program with abstracts*, **23**, A186.

Bortolotti, V., Nicolae, I., Marroni, I., Pandolfi, L., Principi, G., and Saccani, E. (2002) Geological and petrological evidences for Jurassic association of ophiolites and Island arc volcanics in the South Apuseni Mountains (Romanian Carpathians). *International Geology Review*, **44**, 938–955.

Cathelineau, M. (1988) The chlorite and illite geotherm-ometers. *Chemical Geology*, **70**, 182–182.

Chipera, S.J. and Apps, J.A. (2001) Geochemical stability of natural zeolites. Pp. 117–161 in: *Natural Zeolites: Occurrence, Properties, Applications* (D.L. Bish and D.W. Ming, editors). Reviews in Mineralogy and Geochemistry, **45**, Mineralogical Society of America, Washington, D.C.

Cho, M., Liou, J.G., and Maruyama, S. (1986) Transition from the zeolite to prehnite-pumpellyite facies in the Karmutsen Metabasites, Vancouver Island, British Columbia. *Journal*

of Petrology, **27**, 467–494.
Cho, M. (1991) Zeolite to prehnite-pumpellyite facies metamorphism in the Toa Baja Drill Hole, Puerto Rico. *Geophysical Research Letters*, **18**, 525–528.
Coombs, D.S. (1960) Lower grade metamorphic facies in New Zealand. *21st International Geological Congress, Copenhagen, 1960*, **13**, 339–351.
Coombs, D.S., Nakamura, Y., and Vuagnat, M. (1976) Pumpellyite-actinolite facies schist of the Tevayanne formation, near Loeche, Switzerland. *Journal of Petrology*, **17**, 440–471.
Day, H.W. and Springer, R.K. (2005) The first appearance of actinolite in the prehnite-pumpellyite facies, Sierra Nevada, California. *The Canadian Mineralogist*, **43**, 89–101.
Dekayir, A., Amouric, M., and Olives, J. (2005) Clay minerals in hydrothermally altered basalts from Middle Atlas, Morocco. *Clay Minerals*, **40**, 67–77.
Digel, S. and Ghent, E.D. (1994) Fluid-mineral equilibria in prehnite-pumpellyite to greenschist facies metabasites near Flin Flon, Manitoba, Canada: implications for petrogenetic grids. *Journal of Metamorphic Geology*, **12**, 467–477.
Drief, A. and Schiffman, P. (2004) Very low-temperature alteration of sideromelane in hyaloclastites and hyalotuffs from Kilauea and Mauna Kea volcanoes: Implications for the mechanism of palagonite formation. *Clays and Clay Minerals*, **52**, 622–634.
Ellero, A., Leoni, L., Marroni, M., Nicolae, I., Pandolfi, L., and Sartori, F. (2002) Deformation and metamorphism in the Feneş Nappe (southern Apuseni Mountains, Romania). *Comptes Rendus Geoscience*, **334**, 347–354.
Essene, E.J. and Peacor, D.R. (1995) Clay mineral thermometry: A critical perspective. *Clays and Clay Minerals*, **43**, 540–553.
Evarts, R.C. and Schiffman, P. (1983) Submarine hydrothermal metamorphism of the Del Puerto ophiolite, California. *American Journal of Science*, **283**, 289–340.
Fridriksson, T., Neuhoff, P.S., Arnorsson S., and Bird, D.K. (2001) Geological constraints on the thermodynamic properties of the stilbite–stellerite solid solution in low-grade metabasalts. *Geochimica et Cosmochimica Acta*, **65**, 3993–4008.
Giorgetti, G., Monecke, T., Kleeberg, R., and Hannington, M.D. (2006) Low-temperature hydrothermal alteration of silicic glass at the Pacmanus hydrothermal vent field, Manus basin: An XRD, SEM and AEM-TEM study. *Clays and Clay Minerals*, **54**, 240–251.
Giorgetti, G., Monecke, T., Kleeberg, R., and Hannington, M.D. (2009) Low-temperature hydrothermal alteration of trachybasalt at Conical Seamount, Papua New Guinea: Formation of smectite and metastable precursor phases. *Clays and Clay Minerals*, **57**, 725–741.
Hoeck, V., Ionescu, C., Balintoni, I., and Koller, F. (2009) The Eastern Carpathians "ophiolites" (Romania): Remnants of a Triassic ocean. *Lithos*, **108**, 151–171.
Istrate, G. (1980) The nature and composition of Romanian zeolites. *Anuarul Institutului de Geologie si Geofizica*, **56**, 143–152.
Inoue, A. and Utada, M. (1991) Smectite-to-chlorite transformation in thermally metamorphosed volcanoclastic rocks in the Kamikita area, northern Honshu, Japan. *American Mineralogist*, **76**, 628–640.
Ionescu, C., Hoeck, V., Tomek, C., Koller, F., Balintoni, I., and Besutiu, L. (2009) New insights into the basement of the Transylvanian Depression (Romania). *Lithos*, **108**, 172–191.
Leoni, L., Lezzerini, M., Battaglia, S., and Cavalcante E. (2010) Corrensite and chlorite-rich Chl-S mixed layers in sandstones from the 'Macigno' Formation (northwestern Tuscany, Italy). *Clay Minerals*, **45**, 87–106.
Liou, J.G. (1979) Zeolite facies metamorphism of basaltic rocks from the East Taiwan ophiolite. *American Mineralogist*, **64**, 1–14.
Liou, J.G., Maruyama, S., and Cho, M. (1987) Very low-grade metamorphism of volcanic and volcanoclastic rocks-mineral assemblages and mineral facies. Pp. 59–113 in: *Low-Temperature Metamorphism* (M. Frey, editor). Blackie & Son Ltd., Glasgow, UK, 351 pp.
Marantos, I., Markopoulos, Th., Christidis, G.E., and Perdikatsis, V. (2008) Geochemical characteristics of the alteration of volcanic and volcaniclastic rocks in the Feres Basin, Thrace, NE Greece. *Clay Minerals*, **43**, 575–595.
Maruyama, S. and Liou, J.G. (1988) Petrology of Franciscan metabasites along the jadeite-glaucophane type facies series, Cazadero, California. *Journal of Petrology*, **29**, 1–37.
Miyahara, M., Kitagawa, R., and Uehara, S. (2005) Chlorite in metabasites from the Mikabu and north Chichibu belts, southwest Japan. *Clays and Clay Minerals*, **53**, 466–477.
Merriman, R.J. and Peacor, D.R. (1999) Very low grade metapelites: Mineralogy, microfabrics and measuring reaction progress. Pp. 10–60 in: *Low-Grade Metamorphism* (M. Frey and D. Robinson, editors). Blackwell Science Ltd., Oxford, UK.
Meunier, A., Mas, A., Beaufort, D., Patrier, P., and Dudoignon, P. (2008a) Clay minerals in basalt-hawaiite rocks from Mururoa atoll (French Polynesia). I. Mineralogy. *Clays and Clay Minerals*, **56**, 711–729.
Meunier A., Mas, A., Beaufort, D., Patrier, P., and Dudoignon, P. (2008b) Clay minerals in basalt-hawaiite rocks from Mururoa atoll (French Polynesia). II. Petrography and geochemistry. *Clays and Clay Minerals*, **56**, 730–750.
Miron, D. (2006) Preliminary mineralogical aspects on some zeolites from the Mureş Valley, Romania. 3rd "Mineral Science in the Carpathians" International Conference. *Acta Mineralogica-Petrographica*, Abstract Series **5**, Szeged, Hungary.
Muñoz, M., Aguirre, L., Vergara, M., Demant, A., Fuentes, F., and Fock, A. (2010) Prehnite-pumpellyite facies metamorphism in the Cenozoic Abanico Formation, Andes of central Chile (33º50'S): chemical and scale controls on mineral assemblages, reaction progress and the equilibrium state. *Andean Geology*, **31**, 54–77.
Neuhoff, P.S. and Ruhl, L.S. (2006) Mechanisms and geochemical significance of Si-Al substitution in zeolite solid solutions. *Chemical Geology*, **225**, 373–387.
Neuhoff, P.S., Rogers, K.A., Stannius, L.S., Bird, D.K., and Pedersen, A.K. (2006) Regional very low-grade metamorphism of basaltic lavas, Disko-Nuussuaq region, west Greenland. *Lithos*, **92**, 33–54.
Nicolae, I. (1994) Guide to excursion. Forth Day: The ophiolitic rocks from Mureş Valley. *ALCAPA II*, **75**, 136–145.
Passaglia, E. and Sheppard, R.A. (2001) The crystal chemistry of zeolites. Pp. 69–92 in: *Natural Zeolites: Occurrence, Properties, Applications* (D.L. Bish and D.W. Ming, editors). Reviews in Mineralogy and Geochemistry, 45, Mineralogical Society of America, Washington, D.C.
Rieder, M., Cavazzini, G., D'yakonov, Y.S., Frank-Kamenetskii, V.A., Gottardi, G., Guggenheim, S., Koval, P.V., Mueller, G., Neiva, A.M.R., Radoslovich, E.W., Robert, J-L., Sassi, F.P., Takeda, H., Weiss, Z., and Wones, D.R. (1998) The nomenclature of the micas. *The Canadian Mineralogist*, **36**, 41–48.
Reynolds, R.C. Jr. (1988) Mixed layer chlorite minerals. Pp. 601–629 in: *Hydrous Phyllosilicates* (S.W. Bailey, editor). Reviews in Mineralogy, **19**. Mineralogical Society of America, Washington, D.C.
Robinson, D., Bevins, R.E., and Rowbotham, G. (1993) The characterization of mafic phyllosilicates in low-grade

metabasalts from eastern North Greenland. *American Mineralogist*, 78, 377–390.

Robinson, D. and Bevins, R.E. (1994) Mafic phyllosilicates in low-grade metabasites. Characterization using deconvolution analysis. *Clay Minerals*, **29**, 223–237.

Robinson, D., Bevins, R.E., and Rubinstein, N. (2005) Subgreenschist facies metamorphism of metabasites from the Precordillera terrane of western Argentina; constraints on the later stages of accretion onto Gondwana. *European Journal of Mineralogy*, **17**, 441–452.

Saccani, E., Nicolae, I., and Tassinari, R. (2001) Tectono-magmatic setting of the Jurrasic ophiolties from the South Apuseni Mountains (Romania): petrological and geochemical evidence. *Ofioliti*, **26**, 9–22.

Savu, H. (1983) Goetectonic and magmatic evolution of the Mureş zone (Apuseni Mountains) – Romania. *Anuarul institutului de Geologie si Geofizică*, **61**, 253–262.

Savu, H. (1996) Metamorphic and metasomatic processes in the Mureş Zone Alpine ophiolites and the related formations: a synthesis aproach. *Analele Universitatii din Bucuresti*, **49**, 3–14.

Savu, H. and Udrescu, C. (1996) The ophiolites of the Mureş couloir between Căpîlnaş and Tisa (Mureş Zone). *Romanian Journal of Petrology*, **77**, 61–70.

Savu, H., Lemne, M., Romanescu, O., Stoian, M., and Grabari, G. (1986) Distribution of U, Th, K, REE and other trace elements in island arc volcanics and some ophiolites from Vata-Vorta-Vălisoara region (Mureş zone). *Dări de seamă ale Institutului de Geologie si Geofizică*, **70–71**, 431–452.

Savu, H., Stoian, M., Tiepac, I., and Grabari, M. (1994) Petrological significance of REE, U, Th, Rb, Sr, Hf and the Sr 87/86 in the basaltic complex of the Mureş zone. *Romanian Journal of Petrology*, **76**, 77–84.

Schiffman, P. and Fridleifsson, G.O. (1991) The smectite to chlorite transition in drillhole NJ-15, Nesjavellir geothermal field, Iceland: XRD, BSE and electron microprobe investigations. *Journal of Metamorphic Geology*, **9**, 679–696.

Schiffman, P. and Staudigel, H. (1995) Hydrothermal alteration of a scamount complex on La Palma, Canary Islands: implications for metamorphism in accreted terranes. *Geology*, **22**, 151–54.

Schmidt, S.Th. and Robinson, D. (1997) Metamorphic grade and porosity and permeability controls on mafic phyllosilicate distributions in a regional zeolite to greenschist facies transition of the North Shore Volcanic Group, Minnesota. *GSA Bulletin*, **109**, 683–697.

Shau, Y.H. and Peacor, D.R. (1992) Phyllosilicates in hydrothermally altered basalt from DSDP Hole 504B, leg 83. A TEM and AEM study. *Contributions to Mineralogy and Petrology*, **112**, 119 – 133.

Shau, Y.H., Peacor, D.R., and Essene, E.J. (1990) Corrensite and mixed-layer chlorite/smectite in metabasalt from northern Taiwan: TEM/AEM, EMPA, XRD, and optical studies. *Contributions to Mineralogy and Petrology*, **105**, 123–142.

Springer, R.K., Day, H.W., and Beiersdorfer, R.E. (1992) Prehnite-pumpellyite to greenschist facies transition, Smartville Complex, near Auburn, California. *Journal of Metamorphic Geology*, **10**, 147–170.

Treacy, M.M.J., Higgins, J.B., and von Ballmoos, R. (2001) Collection of Simulated XRD Powder Diffraction Patterns for Zeolites, 4th revised edition. Elsevier, Amsterdam.

Utada, M. (1970) Occurrence and distribution of authigenic zeolites in the Neogene pyroclastic rocks in Japan. *Scientific Papers of the College of General Education, University of Tokyo*, **20**, 191–262.

Utada, M. (2001) Zeolites in hydrothermally altered rocks. Pp. 305–322 in: *Natural Zeolites: Occurrence, Properties, Applications* (D.L. Bish and D.W. Ming, editors). Reviews in Mineralogy and Geochemistry, **45**, Mineralogical Society of America, Washington, D.C.

(*Received 17 January 2011; revised 27 August 2011; Ms. 534; A.E. W. Huff*)